Macromolecules

pubs.acs.org/Macromolecules Article

Pressure-Induced Phase Transitions of Nonionic Polymer Brushes

Samantha Micciulla, Philipp Gutfreund, Matej Kanduč,* and Leonardo Chiappisi*

Cite This: https://doi.org/10.1021/acs.macromol.2c01979 Read Online

ACCESS | Metrics & More | Article Recommendations | Supporting Information

ABSTRACT: While the temperature responsive behavior of nonionic polymers has been extensively studied and is nowadays one of the key mechanisms of smart materials, the pressure response of thin films remains basically unexplored. We investigate the conformational transition of nonionic brushes and semidilute solutions induced by hydrostatic pressure and temperature variations. Interestingly, the pressure−temperature phase diagram for the coil-to-globule transition of brushes, probed by neutron reflectometry, nearly coincides with that in semidilute solutions. We also show that the phase behavior can be understood and predicted with simple thermodynamic concepts employed so far for the denaturation of proteins. Fully atomistic molecular dynamics simulations provide molecular insight into the pressure-responsive behavior. Combining all three approaches allows us to demonstrate that pressure-induced hydration of nonionic polymers at low pressure is universal as it is dictated by water and is polymer-independent. In contrast, the pressure-induced dehydration at high pressure is strongly polymer-specific. The outcomes apply to a wide class of nonionic polymers and can aid the design of responsive coatings with the desired pressure-responsive behavior.

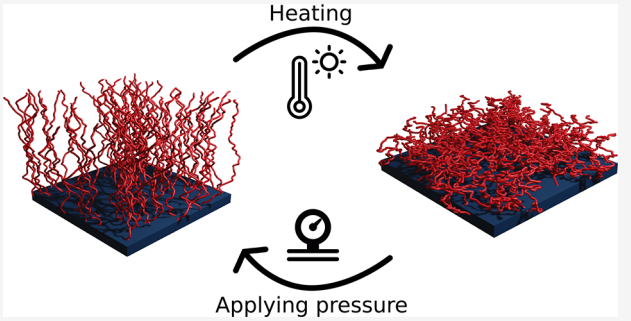

INTRODUCTION

Polymers are key elements in modern material science. Since Leo Hendrik Baekeland prepared the first synthetic polymer, Bakelite, in 1907,[1] tremendous progress in both polymer chemistry and polymer physics has been made. Today, an endless library of polymers adapted to specific needs is available. Moreover, great advancement has been achieved in the preparation of stimuli-responsive, or smart, polymers—which allow the properties of the material to react to changes in the surrounding environment. Such materials are used for very different applications, among which are drug delivery, sensors, actuators, or optoelectronics devices.[2,3]

In most cases, only a thin film of the responsive polymer—the "smart coating"—is sufficient to impart the desired properties to a bulk material. Among the different architectures of such coatings, polymer brushes are widely exploited for applications that require high mechanical stability as well as a rapid and reversible change of the film properties upon application of an external stimulus.[4] One of the most exploited stimuli to trigger structural changes in polymer brushes is temperature, and since the first reports of the thermoresponsive behavior of poly(*N*-isopropylacrylamide) (PNIPAM) in an aqueous environment in the late 1960s,[5,6] PNIPAM-based responsive coatings have emerged as the archetype of thermoresponsive nonionic polymer systems.

The temperature-induced phase transition of PNIPAM, from a swollen and hydrated configuration to a collapsed, dehydrated state, mainly originates from the entropic gain of the disruption of the water network around the polymer chain. Understanding this transition is technically highly relevant, as it is a pillar of the design of thermoresponsive systems.[7] Accordingly, virtually every experimental technique has been employed to study the phase transition of PNIPAM in aqueous solution,[8] e.g., turbidimetry,[9] microcalorimetry,[10,11] scattering methods,[12,13] and computer simulations.[14−16] For what concerns the thermoresponsive behavior of polymer brushes—affected by the crowding of the polymer chains—it is probed by more sophisticated surface-sensitive techniques, such as neutron and X-ray reflectometry,[17,18] quartz-crystal microbalance,[18,19] or atomic force microscopy.[18,19]

However, temperature is not the sole thermodynamic parameter that can be used to control the phase behavior of polymeric systems; the variation of pressure can similarly induce phase transitions. While states with the highest entropy are stabilized at high temperatures, high pressures favor the states with smaller volumes. Changes in both volume and entropy associated with polymer phase transitions in aqueous media are dominated by the properties of hydration water.[20,21] Although pressure effects have been much less studied,[22,23] mainly because of technical limitations, there are at least two main reasons that motivate the use of hydrostatic pressure to

Received: September 28, 2022
Revised: December 13, 2022

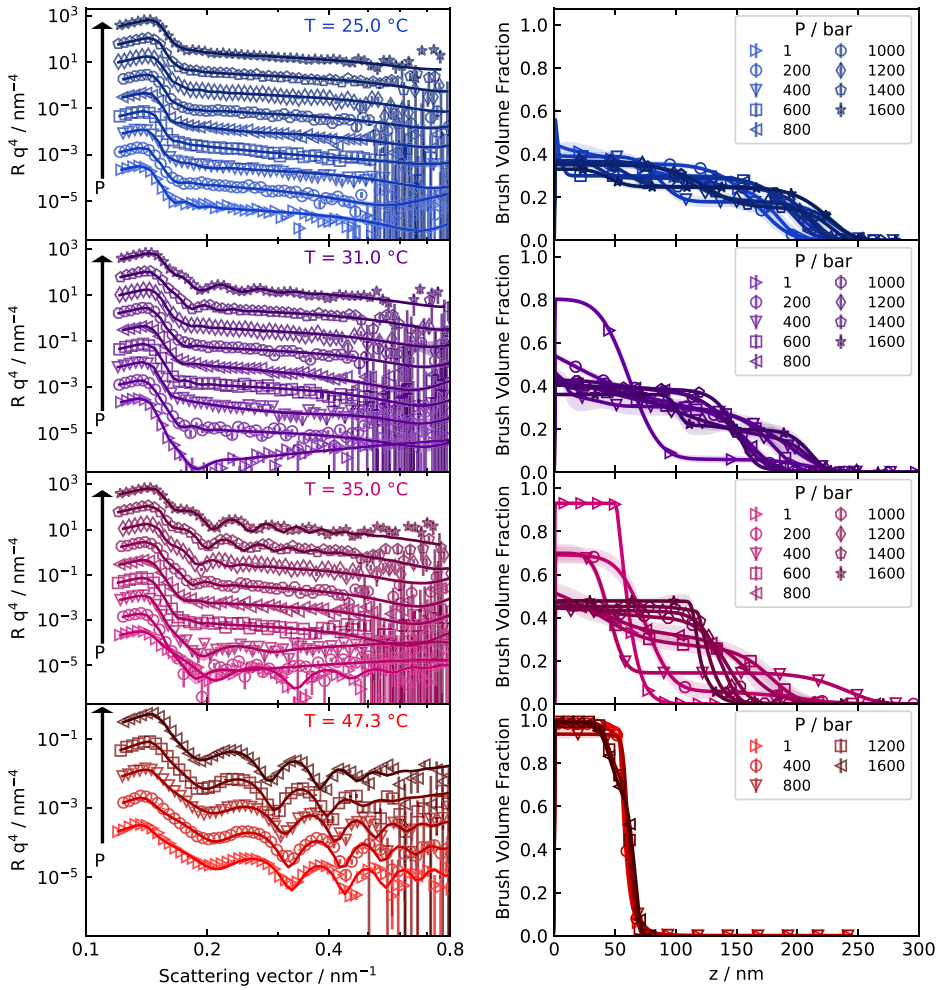

Figure 1. Neutron reflectivity data and analysis. Neutron reflectivity (multiplied by the scattering vector q^4) data of PNIPAM brushes (on the left) and obtained brush volume fraction profiles (on the right). Full lines and shaded areas represent the average value and standard deviation of the obtained volume fraction profile and neutron reflectivity, respectively. Reflectivity data are scaled to improve readability, and arrows indicate increasing pressure. Note the logarithmic scale used for the q-axis of the reflectivity plot.

probe the behavior of polymer systems: (i) the high relevance of high-pressure processing, especially in biotechnology and food science,[24−26] and (ii) the fact that the variation of pressure provides an additional dimension to explore the fundamentals of polymer phase transitions.[13,27] In particular, the combined investigation of temperature and pressure effects is required to fully describe the free energy landscape.

In this work, we present an extensive study of the pressure−temperature phase behavior of PNIPAM brushes in aqueous media. We have combined structural information gained by neutron reflectometry experiments with a thorough investigation of the free-energy landscape determined by calorimetry and volumetry. To support the interpretation of our experimental results, we performed theoretical studies by molecular dynamics simulations, which have provided atomistic insights into the origin of the pressure-induced phase transition. To strengthen the generality of our findings for nonionic polymeric systems, we conducted additional experiments with poly[2-(dimethylamino)ethyl methacrylate] (PDMAEMA) brushes under unprotonated conditions.

RESULTS AND DISCUSSION

Volume Fraction Profiles Resolved by Neutron Reflectometry. The conformation of PNIPAM and PDMAEMA brushes, the latter under nonionic conditions, has been probed as a function of pressure and temperature by neutron reflectivity (NR), which can resolve the volume fraction profile of the brush normal to the substrate with angstrom resolution. The NR data are shown in Figures 1 and S1 for PNIPAM and PDMAEMA brushes, respectively. All experiments were performed in D_2O for PNIPAM and in 25 mM potassium phosphate buffer at pD = $-\log a_{D^+}$ = 8.0 for PDMAEMA, ensuring a degree of ionization of <10%.[28]

The NR curves in Figure 1 clearly show the signature of the swollen-to-collapsed transition in polymer brushes. At low temperatures, the reflectivity data have very few features—typical for highly swollen systems where the scattering length density profile continuously decays toward the value of the solvent.[29] In contrast, curves measured at 31 and 35 °C at high pressure and at 47 °C at any investigated pressure value show marked oscillations, characteristic of a sharp interface between the polymer film and the solvent. The same trend can also be observed in the PDMAEMA data shown in Figure S1.

The NR data analysis enables a precise determination of the polymer brush volume fraction profile, thus allowing us to detect changes in polymer conformation upon variations of temperature and pressure. The volume fraction profiles of the PNIPAM brushes, obtained by fitting the neutron reflectom-

https://doi.org/10.1021/acs.macromol.2c01979
Macromolecules XXXX, XXX, XXX−XXX

etry data with a two-region analytical model, are shown in Figure 1. The fitting procedure is constrained so that the amount of polymer on the substrate is constant and equal to the amount determined by multiangle optical ellipsometry (data provided in the Supporting Information). The uncertainty in the volume fraction profiles was estimated by bootstrap error analysis. Further details on the modelization of the neutron reflectometry data are given in the Supporting Information.

In agreement with the qualitative changes of the NR curves, the quantitative analysis, resulting in the volume fraction profiles shown in Figure 1, clearly shows the swollen-to-collapsed transition. In particular, at low temperature, the brush exhibits a continuously decreasing polymer concentration, vanishing at the brush/solvent interface. In contrast, collapsed brushes show a sharp interface between the polymer film and the solvent, which translates to pronounced oscillations in the NR curves. A qualitative interpretation of the volume fraction profiles indicates that the transition from a swollen brush, with a parabolic profile, toward the collapsed state passes by an intermediate structure, which is dehydrated in the proximity of the substrate and more hydrated in its outermost region—in agreement with previous studies.[30,31] To highlight the effect of temperature at different pressures, selected NR data and resulting brush volume fraction profiles are shown in Figure S2.

Using these volume fraction profiles, we extracted physicochemical parameters such as the brush hydration, thickness, and roughness (using eqs 5−7), which are shown in Figure 2 for PNIPAM brushes and in Figure S6 for PDMAEMA. They clearly indicate that increasing the temperature causes the collapse of the polymer brush, resulting in a lower degree of hydration and smaller brush thickness. In contrast, increasing the hydrostatic pressure in the system causes the brush to swell, as indicated by increase of the degree of hydration and brush thickness. The phenomenon is particularly evident at 31 and 35 °C for PNIPAM brushes and at all investigated temperatures for PDMAEMA brushes. Interestingly, the maximal thickness and degree of hydration of PNIPAM brushes occur between 600 and 800 bar for curves recorded at 31 and 35 °C. The pressure-induced swelling observed here is in agreement with studies on aqueous solutions of PNIPAM, whereby it was shown that up to moderate pressures of 1000 bar the solubility of PNIPAM increases with increasing pressure.[32,33]

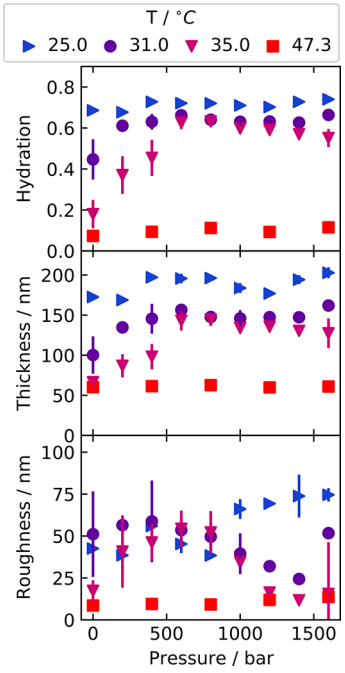

Figure 2. Structural parameters obtained for PNIPAM brushes. From top to bottom: the degree of hydration of the brush, the brush thickness, and the brush roughness as a function of hydrostatic pressure and temperature. The parameters are obtained from the fit using a two-region analytical function to describe the brush volume fraction profile. See the Materials and Methods section for further details.

It is important to mention that given the continuous dehydration of the brush with temperature and pressure, the definition of a "collapsed" or "swollen" brush might hold some ambiguity. However, self-consistent field theory predicts that in good solvent conditions the polymer volume fraction profile continuously decreases, vanishing at the brush/water interface, whereas in poor solvent conditions the volume fraction profile exhibits an abrupt decrease, whereby the polymer concentration at the brush/water interface equals that of polymer globules in solution.[34] Following the criteria of having a sharp brush/water interface, the brushes at 35 °C and 1 bar, at 35 °C above 1200 bar, and all brushes at 47 °C can be considered as collapsed. For the brushes at 35 °C, comparing their states at 1 and 1600 bar (Figure S9), an additional effect of the applied pressure can be observed: while the brush exhibits a sharp profile in both cases, characteristic of poor solvent conditions, the inner part of the brush is significantly more hydrated at high pressure than at low pressure. This finding is also in line with numerous observations of polymer solutions in which polymer globules are much more hydrated at high pressures than at low ones.[27,35,36] Specifically, while at 35 °C and ambient pressure the inner part of the brush is almost dehydrated, at 1600 bar, it features a water content of approximately 55 vol %, corresponding to approximately 7 water molecules per PNIPAM monomer.

Free Energy Landscape Determination. To fully understand the pressure- and temperature-induced swelling/deswelling of the polymer brushes, a quantitative determination of the free energy landscape is necessary. From a thermodynamic perspective, the temperature- and pressure-dependent phase behavior of polymer solutions can be described with the Hawley formalism, originally developed to illustrate the process of protein denaturation.[23,37] In detail, the pressure−temperature phase diagram is predicted based on the simple assumption that the polymer exists in two states only—swollen and collapsed—and that the transition occurs when the free energy difference (ΔG) between the two states is zero. The free energy landscape can be drawn if all the derivatives of the free energy change are known:[23]

$$\Delta G(T, P) = \Delta G_0 - \Delta S(T - T_0) + \Delta V(P - P_0) + \Delta\alpha(P - P_0)(T - T_0) - \Delta C_p\left[T\left(\ln\frac{T}{T_0} - 1\right) + T_0\right] - \frac{\Delta\kappa}{2}(P - P_0)^2 + \ldots \quad (1)$$

where the prefactors are differences between the collapsed and swollen state in entropy ($\Delta S = \Delta(\partial G/\partial T)_P$), volume ($\Delta V =$

https://doi.org/10.1021/acs.macromol.2c01979
Macromolecules XXXX, XXX, XXX−XXX

$\Delta(\partial G/\partial P)_T$), thermal expansion factor ($\Delta\alpha = \Delta(\partial V/\partial T)_P$), heat capacity ($\Delta C_p = T\Delta(\partial S/\partial T)_P$), and isothermal compressibility factor ($\Delta\kappa = -\Delta(\partial V/\partial P)_T$). The offset ΔG_0 is the free energy difference between the two states at arbitrarily chosen coordinates T_0 and P_0. For the pleasure of symmetry and to simplify the analysis of the solutions of eq 1, the term $T[\ln(T/T_0) - 1] + T_0$ can be approximated to $(T - T_0)^2/(2T_0)$ for $T \sim T_0$.

The coexistence line, i.e., the pairs of values of T and P where $\Delta G(T, P) = 0$, can be calculated if the thermodynamic parameters in eq 1 are known. Regrettably, the required parameters associated with the swelling/deswelling of polymer brushes grafted on planar substrates are not experimentally accessible. Herein, to overcome this intrinsic limitation of thin films, we opted for using the parameters determined in aqueous solutions instead. In detail, all the thermodynamic parameters in eq 1 were determined for 3 wt % PNIPAM and PDMAEMA in a semidilute solution by means of differential scanning calorimetry, density, and sound velocity measurements (see the Supporting Information for a full discussion) and are given in Table 1. The values are in good agreement

Table 1. Thermodynamic Parameters Associated with the Dehydration Process Obtained from the Analysis of the Calorimetric and Volumetric Experiments Performed on 3 wt % PNIPAM in D_2O or PDMAEMA Solutions in a 25 mM Phosphate Buffer in D_2O at pD 8, Respectively[a]

		PNIPAM	PDMAEMA
T_c	°C	34.9	39.1
ΔH	kJ mol^{-1}	7.29(5)	3.28(2)
ΔS	J K^{-1} mol^{-1}	23.7(3)	10.5(1)
ΔC_p	J K^{-1} mol^{-1}	−110(1)	−30(4)
ΔV	cm^3 mol^{-1}	2.5(8)	1.4(7)
$\Delta\kappa$	10^{-8}cm^3 Pa^{-1} mol^{-1}	1.5(4)	0.8(9)
$\Delta\alpha$	10^{-2}cm^3 K^{-1} mol^{-1}	4(2)	1.8(5)

[a]Values refer to ambient pressure and transition temperature indicated as T_c. Data are reported per mole of monomer. Values in parentheses are uncertainties on the last significant digit at the given transition temperature.

with the literature[10,11,39] and can be used to describe the free energy landscape, including the swollen−collapsed state coexistence line, of a PNIPAM solution. The predicted coexistence line is compared to the experimentally determined phase boundary for a 3 wt % PNIPAM solution, determined previously,[32,38] as shown in Figure 3a.

While there are a few thermodynamic predictions of the $P-T$ phase diagram of proteins[40,41] and attempts to extract thermodynamic quantities from $P-T$ phase diagrams of polymer solutions,[42−44] to the best of our knowledge this is the first time that an experimental $P-T$ phase diagram of polymer solutions is compared with predictions made from calorimetric and volumetric data. A surprisingly good match can be seen between the predicted coexistence line (i.e., where $\Delta G = 0$) and the experimental data, despite the strong assumption of a two-state system. The deviations at high pressures can be ascribed to the two-state assumption and to neglecting higher-order terms in eq 1.

The positive value of ΔS and the negative value of ΔC_p indicate that the temperature-induced collapse is driven by the entropic gain from the release of hydration water of PNIPAM and PDMAEMA chains, in agreement with numerous previous

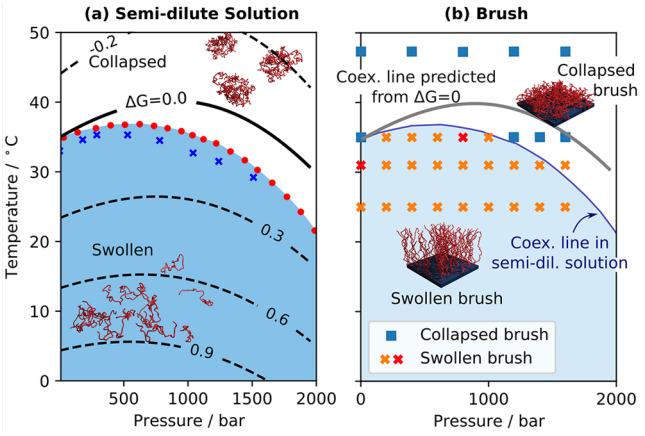

Figure 3. Phase diagrams of PNIPAM in semidilute solution and grafted on planar substrates. (a) Pressure−temperature phase behavior of a 3 wt % PNIPAM semidilute solution in D_2O. Red points and blue crosses indicate experimentally determined phase boundaries as reported in refs 32 and 38, respectively. The contour lines are isoenergetic lines of fixed ΔG (values given in kJ mol^{-1}), calculated with eq 1 using the parameters determined by calorimetry and volumetry. (b) Pressure−temperature phase behavior of PNIPAM brushes in water. Squares and crosses indicate $P-T$ coordinates for collapsed and swollen brushes, respectively (see text for definitions). For the sake of comparison, the experimentally determined coexistence line in the semidilute solution is drawn. The two red crosses indicate the $P-T$ coordinates for PNIPAM brushes under the following conditions: (31 °C, 1 bar) and (35 °C, 800 bar), which are equidistant from the coexistence line and whose volume fractions are compared later in the text.

studies.[45,46] In contrast, the pressure-induced swelling at low to intermediate pressure is due to the positive value for the volume of collapse (+2.5 and +1.4 cm^3 per mole of monomeric units of PNIPAM and PDMAEMA, respectively), also in agreement with the results published by other authors.[44] The pressure-induced collapse at high pressures is finally dictated by the positive change in the compressibility factor of $\Delta\kappa = 1.5 \times 10^{-8}$ and 0.8×10^{-8} cm^3 Pa^{-1} per mole of PNIPAM and PDMAEMA monomeric units, respectively. The molecular origin of the signs of the ΔV and $\Delta\kappa$ will be discussed later in the text with the insights from molecular dynamics simulations.

As mentioned above, calorimetric and volumetric experiments allowed us to predict the $P-T$ phase behavior of polymer semidilute solutions. For the case of PNIPAM, as shown in Figure 3b, the phase behavior of the polymer brushes follows very closely that of the semidilute solutions, and the calculated coexistence line matches well the experimental points. This result implies that the brush-specific contributions to the system's free energy—arising mainly from the conformational constraints due to covalent anchoring—are negligible compared to the polymer−solvent contributions. Importantly, this finding is also of very high technical relevance, as it suggests that the $P-T$ phase behavior of polymer brushes—accessible by challenging experiments only—can be predicted from a dilute solution of the same polymer by using easily accessible laboratory-scale equipment (calorimetry, volumetry, and sound-velocity experiments).

In addition to the technical relevance of this comparison, combining the information from the free energy landscape and the reflectometry structural study allows us to disentangle pressure- and temperature-related effects. In particular, we aim at comparing the brush volume fraction profile recorded at

https://doi.org/10.1021/acs.macromol.2c01979
Macromolecules XXXX, XXX, XXX−XXX

different pressures and temperatures that are equally distant from the coexistence line. Accordingly, the profiles recorded at 31 °C and 1 bar are compared with those recorded at 35 °C and 800 bar (indicated by red crosses in Figure 3). In both cases, the brush is in the swollen state with the free energy of collapse of approximately $\Delta G \approx 90$ J mol^{-1} (see Figure 4).

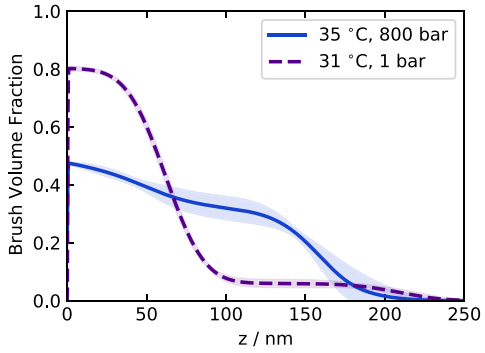

Figure 4. Brush volume fraction profiles of PNIPAM at 31 °C and 1 bar and at 35 °C and 800 bar.

Interestingly, their volume fraction profiles are significantly different. At ambient pressure, the brush profile resembles a typical parabolic density profile—a signature of polymer brushes immersed in a good low-molecular-weight solvent. At 800 bar, however, the density profile has a more sigmoidal shape, with a sharper boundary between the regions, despite the higher overall brush hydration. A similar situation is observed for the PNIPAM brush in the collapsed state at 35 °C and at 1 and 1600 bar, also equidistant from the coexistence free energy line, with a ΔG of collapse of −10 J mol^{-1} (see Figure S9). The brush volume fractions feature sharp sigmoidal profiles in both of these two states, but with very different hydration levels: the brush is nearly dry at ambient pressure, whereas it is substantially hydrated at 1600 bar. The higher hydration of the polymer brushes at high pressure, also in the collapsed state, could be due to a change in the solvent quality of water at higher pressures, resulting in a changed balance between "hydrophilic" water, acting as a typical good solvent and breaking bonds between monomers and "hydrophobic" water, which is swelling the polymer without triggering significant conformational changes. The origin of this "bipolarity" of water interactions at elevated pressures could be either a shifted balance of hydrogen bonds between water molecules and monomers, evoked later in the text by computer simulations, or a changed balance of water molecules being close to hydrophilic and hydrophobic parts of the polymer as reported by Tavagnacco et al.[27]

Very interestingly, by inspecting the $P-T$ phase diagram of different nonionic polymers solutions, Reinhardt et al.[47] pointed out that the initial slope of the coexistence line is *independent* on the nature of the polymer, being approximately $dp/dT \approx 100$ bar K^{-1}. The same result is obtained from the ratio $\Delta S/\Delta V$ determined by calorimetric and volumetric analysis in this work (90 ± 30 and 80 ± 40 bar K^{-1} for PNIPAM and PDMAEMA, respectively). This finding hints toward a polymer-unspecific mechanism for the collapse of polymer brushes and the phase separation of polymer solutions. It further indicates that the origin resides in the behavior of water, which is probed in detail by fully atomistic molecular dynamic (MD) simulations of PNIPAM hereafter.

With the Hawley free-energy analysis (eq 1), we related the reentrant pressure-response behavior with increases in volume ($\Delta V > 0$) and compressibility ($\Delta\kappa > 0$) coefficient after the collapse of both polymer brushes. In the final step of this study, we aim to understand why the system expands and its compressibility increases in the collapsed state.

Insights from Simulations. All-atom simulations have been widely used to study various thermoresponsive polymers, particularly PNIPAM. Yet, it may be surprising that MD studies of hydrostatic pressure effects on polymer transitions remain scarce and mainly limited to the single-chain level.[27,48] Here, we used MD simulations to gain molecular-level insight into the effect of hydrostatic pressure on the polymer phase transition to explain the experimental results. Specifically, we investigate the reasons behind $\Delta V > 0$ and $\Delta\kappa > 0$ of the PNIPAM phase transition.

Because atomistic modeling does not allow simulations of the entire brush because of prohibitively large size and time scales associated with the transition, we adopt the modeling approach established before,[49,50] in which the swollen and collapsed states are treated separately, as shown in Figure 5.

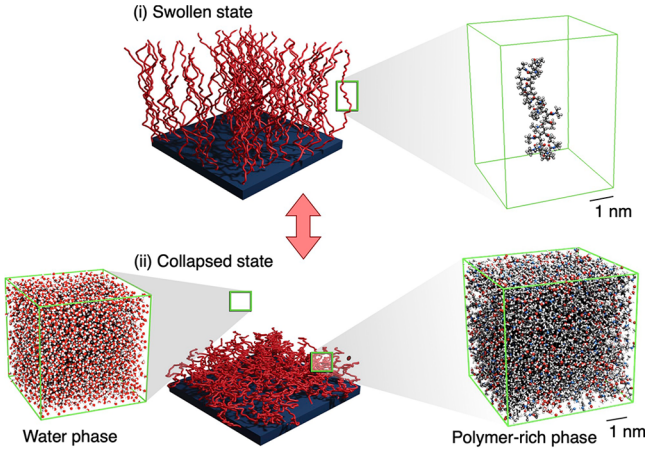

Figure 5. Brush states and simulation setup. (i) The swollen state (schematic, left), where adjacent polymer chains are far apart, is simulated as a stretched and restrained PNIPAM chain in water (MD snapshot, right; water molecules not shown for visibility). (ii) The collapsed state (schematic, middle) is modeled separately as a dense aggregate of PNIPAM chains with water (MD snapshot, right) and a bulk water phase (MD snapshot, left).

The swollen state is modeled as a single stretched and restrained polymer chain in a water box (Figure 5i), corresponding to excessive hydration where neighboring chains are sufficiently far apart and do not interfere with one another. The collapsed state consists of a polymer-rich phase, modeled as a partially hydrated aggregate of polymeric chains, and a bulk water phase, which corresponds to the released water. Both phases are simulated separately (Figure 5(ii)). The simulations of the collapsed state were performed in a range of hydration n_w (water molecules per PNIPAM monomeric unit) of 0.7−1.7, corresponding to a polymer volume fraction of 78−90 %. The reader is referred to previous publications[49,50] and to the Methods section of this paper for further details on the calculation of the volume and compressibility differences.

In agreement with the experimental results, the simulations exhibit a positive volume difference ΔV per monomer between the collapsed and swollen states (shown in Figure 6a, top),

https://doi.org/10.1021/acs.macromol.2c01979
Macromolecules XXXX, XXX, XXX−XXX

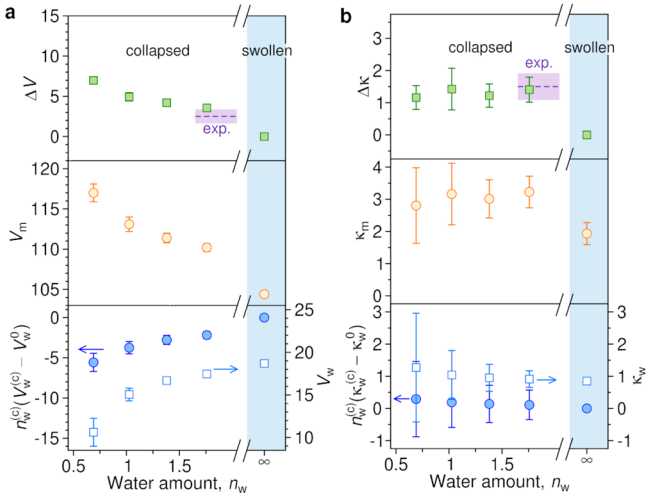

Figure 6. Volume and compressibility changes as obtained from MD simulations. Changes in (a) the volume (in cm^3 mol^{-1}) and (b) compressibility factor (in 10^{-8} cm^3 Pa^{-1} mol^{-1}) from the MD simulations as a function of the number of water molecules per monomer. The data points at $n_w = \infty$ correspond to the swollen state. Top panels: total difference in the volume and compressibility per monomer between the collapsed and swollen states. The purple dashed lines denote the experimental values (see Table 1). Middle panels: partial monomer volume and compressibility. Bottom panels: partial water volume and compressibility (right scale) and the water contributions to the volume and compressibility change (left scale).

which further increases with dehydration (i.e., with decreasing n_w). In the middle and bottom panels, the change in volume (ΔV) is decomposed into partial monomer (V_m) and water (V_w) volumes (see eq 12). The partial monomer volume increases with dehydration, whereas the partial water volume and its contribution decrease, which is typical for nonideal mixing of liquids. Commonly, mixing water with other miscible simple liquids (e.g., alcohols, ethers, and other polar organic substances) results in a smaller volume of the mixture than the sum of volumes of the two pure liquids. A negative excess volume of liquid mixtures turns out to be quite general because smaller molecules can fill up tiny, submolecular voids between larger molecules.[51−55]

The question remains whether the collapsed state of PNIPAM contains only more small subatomic voids than the swollen state or also larger, molecular-size cavities, as in hydrophobic interiors of some proteins.[56−58] To answer this, we analyzed the occurrence of voids (described as empty grid voxels in the simulation box) in both modeled states (shown in Figure S13). The outcomes do not indicate noteworthy cavities of at least the water molecule's size. There is also no significant difference in the frequency of small voids between the two states, which rules out the cavity formation as a cause of volume expansion after the collapse. Instead, the collapsed PNIPAM phase remains compact and essentially homogeneous on the molecular level, in contrast to folded proteins. Moreover, we also examined whether branched PNIPAM chains undergo notable conformation changes that could contribute to the difference in volume. We thus analyzed the extension of side chains from the backbone but found only minor differences between both states, which cannot be attributed to the observed volume change (see Text S6 in the Supporting Information). We conclude that the PNIPAM transition follows the common principles of nonideal mixing of simple liquid mixtures. The volume difference emerges from tiny subatomic voids in the collapsed (unmixed) state, which are filled up by water molecules in the swollen (mixed) state. On the other hand, this points to a different nature of PNIPAM from polypeptides, and thus using PNIPAM as a model surrogate for proteins, sometimes proposed because of the similar chemical structure, should be taken with care, in particular when dealing with pressure effects.

We now address the second question: Why is the collapsed state of PNIPAM more compressible than the swollen one; that is, why is $\Delta\kappa > 0$? The MD result (Figure 6b; top panel) for $\Delta\kappa$ is in excellent agreement with the experiment (dashed purple line) and does not significantly depend on hydration. Simulations further suggest that monomers (middle panel) contribute the major part to $\Delta\kappa$, whereas the water contribution (bottom panel), albeit very noisy, is small. The finding that water does not contribute to the compressibility change is not immediately obvious, as it is known that water bound to hydrophobic entities has a different compressibility than bulk water. Namely, water is less compressible when hydrating small solutes and more compressible at larger ones.[59−61] A recent MD study showed that the crossover between the two hydration regimes of a generic hydrophobic polymer occurs for a polymer diameter of 0.7 nm where the bound water is as compressible as bulk water.[62] In fact, this crossover value is close to the effective PNIPAM diameter of 1 nm,[50] which may explain why water compressibility does not change after the collapse in our system. Thus, the higher compressibility of the collapsed PNIPAM state originates from more compressible polymer chains.

In general, low compressibility is associated with attractive interactions between the molecules, which give rise to a more rigid local structure.[63] An important player in structural rigidity and hence compressibility is the hydrogen-bond (HB) network. Specifically, organic liquids that form HBs (e.g., alcohols, acetates, and ketones) are less compressible than liquids of similar molecular structure without HB-forming groups (e.g., alkanes), which are held together only by weaker and softer dispersion interactions.[63,64] We expect that the HB network of the polymer changes significantly after the collapse, which can be easily examined in simulations.

The analysis of the simulation trajectories implies a significant loss of HBs between the polymer and water upon collapse, counteracted by a slight formation of intermolecular (polymer−polymer) HBs (shown in Figure 7; see the Supporting Information for a description). On the other hand, the released water molecules almost completely compensate for the lost water−polymer HBs by forming new water−water HBs in the bulk phase. Consequently, the net effect is that the total number of HBs remains nearly unchanged. The collapse only redistributes HBs, depriving the polymer and enriching the water phase. Because the collapsed polymer is involved in fewer HBs, and therefore the polymer−polymer interactions become softer (less directional and less specific), the polymer phase is more compressible than the swollen phase (Figure 6b).

Overall, MD simulations suggest that the dehydration mechanism of PNIPAM polymer does not feature a complex supramolecular structure, such as cavity formation, conformational changes of monomers, or a net change in the number of HBs. Volume expansion follows the principles of water mixtures with simple organic liquids, and the higher compressibility of the collapsed state can be explained by the

https://doi.org/10.1021/acs.macromol.2c01979
Macromolecules XXXX, XXX, XXX−XXX

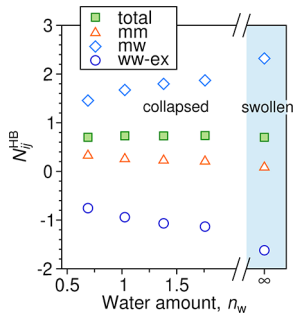

Figure 7. Total number of HBs per monomer, N_{total}^{HB}, as a function of the number of water molecules per monomer and its decomposition into monomer−monomer (mm), monomer−water (mw), and excess water−water (ww−ex) HBs; $N_{total}^{HB} = N_{mm}^{HB} + N_{mw}^{HB} + N_{ww-ex}^{HB}$. The third contribution represents the difference between the number of water−water HBs in the polymer phase and HBs in the bulk−water equivalent. It is defined as $N_{ww-ex}^{HB} = N_{ww}^{HB} - n_w N_{bulk}^{HB}$, where N_{ww}^{HB} is the number of water−water HBs per monomer, n_w is the number of water molecules per monomer, and $N_{bulk}^{HB} = 1.7022(1)$ is the number of HBs per water molecule in bulk water. Error bars are smaller than the symbol sizes.

redistribution of HBs from the polymer to bulk water. This generality possibly explains some observed universal, chemistry-unspecific trends, such as the $\Delta S/\Delta V$ ratio found in experimental studies.[47]

CONCLUSIONS

In summary, the structural behavior of polymer brushes over a wide range of pressure and temperature has been explored using neutron reflectometry. The experiments have revealed that the conformation of PNIPAM and PDAMEMA brushes depends on both pressure and temperature. The transition from a swollen to collapsed brush follows very closely the coexistence line found in semidilute solutions of the same polymer (see Figure 3). Moreover, the phase boundary between the swollen and collapsed state can be predicted with reasonable accuracy by determining the derivatives of the free energy change of collapse up to the second order, i.e., entropy, volume, thermal expansion, heat capacity, and isothermal compressibility.

In agreement with previous studies performed on semidilute solutions,[32,38] we report that increasing temperature reduces the solubility of the investigated polymer brushes in water. In contrast, hydrostatic pressure features a nonmonotonic behavior: it triggers the hydration of the polymer at low pressures and dehydration at high pressures. Through the unprecedented combination of structural studies and the determination of the free energy landscape, we can affirm that the effects of increasing pressure and temperature are not fully orthogonal. In particular, brushes under high hydrostatic pressure exhibit higher hydration close to the substrate, even in the collapsed state, compared to brushes at lower pressure but equidistant from the coexistence line. Moreover, the combination of the thermodynamic investigation with atomistic molecular dynamic simulations provides better insight into the effect of pressure on the phase behavior of polymer brushes and solutions. In particular, the increase of solubility at low and moderate pressures could be ascribed to the unspecific mixing of nonionic solutes with water. These findings explain why the slope of the coexistence line in the $P-T$ phase diagrams is very similar for different nonionic polymers.[47] In contrast, the dehydration of the polymer at high pressure is triggered by the larger compressibility of the collapsed state, owing to the reorganization of hydrogen bonds during the dehydration process. Thus, we can expect the behavior at high pressure to be strongly polymer-specific, whereas the one at low pressure to be dictated mainly by the solvent properties.

By combining neutron reflectometry studies with a throughout thermodynamic characterization, we show that the behavior of polymer systems at pressures up to 2 kbar can be predicted reasonably well with comparably simple techniques (calorimetry and volumetry) using a simple two-state—swollen and collapsed—assumption. This predictive power eases the design of polymer-based additives and coatings for high-pressure applications. From a fundamental science perspective, this work provides valuable insight into the pressure−temperature behavior of PNIPAM and PDMAEMA semidilute solution and brushes. Molecular dynamics simulations support mechanistic conclusions on the universality of the swelling behavior of brushes at low pressure, likely to occur in any nonionic polymer/water mixture. Importantly, fundamental differences are found with respect to the denaturation of proteins, where the presence of cavities largely impacts the ΔV of denaturation.[26,65] Furthermore, the pressure-induced hydration of the polymer chains helps to better understand the extremely low friction coefficients found in synovial fluids and only recently reproduced in polyzwitterionic brushes.[24]

Furthermore, the experimental approach presented in this work, i.e., the combination of structural and thermodynamic studies, may provide further insight into the mechanisms of desolvation also in more complex polymer systems, such as in the presence of salts or low molecular weight organic compounds or in nonaqueous solvents.

MATERIALS AND METHODS

Materials. The silicon substrates (50 × 50 × 10 mm^3) for the preparation of polymer brushes were purchased by Sil'Tronix (Archamps, France). *N*-Isopropylacrylamide (NIPAM, 97%), 2-(dimethylamino)ethyl methacrylate (DMAEMA, 98%, stabilized by monomethyl ether hydroquinone), 2,2′-bipyridyl (bipy, ReagentPlus, ≥99%), *N*,*N*,*N*′,*N*″,*N*″-pentamethyldiethylenetriamine (PMDETA, 99%), copper(I) and copper(II) chloride (CuCl and $CuCl_2$, >99%), and methanol were all purchased from Sigma-Aldrich (France). All reagents were used as received without any further purification. All samples were prepared using D_2O from Eurisotop.

Synthesis of Polymer Brushes. Polymer brushes were grown from silicon wafers (grafting-from approach) by atom transfer radical polymerization (ATRP).[66] Prior to brush synthesis, the substrates were modified by a 2-bromo-2-methyl-*N*-[3-(triethoxysilyl)propyl]-propanamide (BTPAm) monolayer, which self-assembled onto the silicon substrate from a solution in toluene (4 μL of BTPAm in 10 mL of anhydrous toluene, 99.8%) for 18 h. The surface functionalization was performed under argon to ensure a moisture-free atmosphere. After modification, the substrates were rinsed with toluene, blow-dried under nitrogen stream, and stored dry in a desiccator.

For the preparation of PNIPAM brushes, a previously reported protocol was properly adapted to the desired reaction kinetics and sample volume.[67] In brief, a polymerization mixture of 11.32 g of NIPAM in 200 mL of methanol and water (1:1 v/v), 732 μL of triamine ligand (PMDETA), and 0.1 g of CuCl was prepared and degassed by nitrogen bubbling for 40 min. The initiator-modified substrate was soaked in the reaction mixture, and the polymerization was run for 8 min, followed by termination by thorough rinsing in water/methanol mixture and sonication in Milli-Q water. The sample was blow dried under a nitrogen stream and stored in a desiccator.

https://doi.org/10.1021/acs.macromol.2c01979
Macromolecules XXXX, XXX, XXX−XXX

For the preparation of PDMAEMA brushes, the synthetic protocol was adapted from the literature.[68] A suspension of 120 g of the DMAEMA monomer in 180 mL of methanol/water (1:1 v/v) was stirred under a nitrogen atmosphere and added 4.768 g of bipyridine, 1.496 g of CuCl, and 0.101 g of $CuCl_2$. After the complete dissolution of all reagents, the silicon substrate was soaked into the polymerization solution, and the reaction was allowed to run for 5 h. The polymerization was stopped by exposing the samples to oxygen, thoroughly rinsed and sonicated in methanol and water, and finally blow-dried with a nitrogen stream before storage in a desiccator.

From the analysis of the neutron reflectivity curves, the grafting density of the PNIPAM brush is estimated to be between 0.25 and 0.45 chains/nm^2, with a molecular weight of 65−125 kDa. The grafting density of PDMAEMA is estimated to be 0.45−0.65 chains/nm^2 and its molecular weight to 65−120 kDa. See the Supporting Information for full details on the calculation on grafting density and molecular weight.

Methods. *Differential Scanning Calorimetry.* Differential scanning calorimetry was employed to determine the thermal properties of the transition from the swollen to collapsed state of PNIPAM in water and of PDMAEMA in a 25 mM potassium phosphate buffer at pH 8.0. The experiments were performed using a highly sensitive multicell differential scanning calorimeter from TA Instruments. The data were analyzed using the freely available program pyDSC.[69]

Density and Sound-Velocity Measurements. The density and the sound velocity were measured simultaneously as a function of temperature using an Anton-Paar DSA 5000 M apparatus. The data, combined with the heat capacity determined by DSC, were used to calculate the change in volume, compressibility, and thermal expansion, according to the procedure presented in the literature.[40] All details are given in the Supporting Information.

Optical Ellipsometry. The optical thickness of the polymer brushes grafted on silicon blocks was obtained by optical ellipsometry measurements performed using a multiangle optical ellipsometer (Beaglehole Instruments, New Zealand) equipped with a HeNe laser at a wavelength of 632 nm. The angle of incidence was varied between 60° and 80°. The ellipsometric angles Ψ and Δ were fitted using a 4-layer model, consisting of a semi-infinite layer of silicon (with a refractive index of $n = 3.87$), a thin layer of silicon oxide and initiator ($n = 1.46$), a thin layer of a polymer brush, and a semi-infinite layer of air ($n = 1$). The thickness of the silicon oxide/initiator layer of 1.5 nm was determined on a different substrate. To determine the dry thickness of the polymer layer, the measurements were performed under nitrogen flux. The data were analyzed with the freely available python script "pyEllip".[70] Dry thicknesses of 58 nm ($n = 1.46$) and 79 nm ($n = 1.48$) were determined for PNIPAM and PDMAEMA brushes, respectively.

Neutron Reflectometry. Instrumental Details. The high-pressure neutron reflectometry experiments were performed on the time-of-flight (ToF) reflectometer FIGARO[71] at the Institut Laue-Langevin (ILL), Grenoble, France. Using a wavelength band between 2.5 and 20 Å a momentum transfer range of 0.011−0.085 Å^{-1} was accessible by using a single reflection angle of 1°. The momentum transfer resolution was mainly defined by the wavelength resolution of 7.0% (FWHM). The beam footprint on the sample was set to 15 × 30 mm^2, ensuring no overillumation of the sample takes place. The sample was contained in a high-pressure cell for reflectometry described elsewhere.[72] The raw data were normalized to the incident beam spectrum and background corrected by the data reduction software COSMOS.[73]

Full contrast conditions have been achieved by studying hydrogenated polymer brushes immersed in a deuterated solvent, being pure D_2O for PNIPAM and a 25 mM phosphate buffer in D_2O at pH 8.0 for PDMAEMA. The use of a buffer solution for PDMAEMA is justified by the weakly alkaline nature of the polymer, and the choice of pH 8 is the compromise between a sufficient alkaline condition to ensure a low degree of ionization of the polymer of approximately 10%[28] and to avoid alkaline catalyzed hydrolysis of the initiator.

Neutron Reflectometry Data Analysis. The neutron reflectometry data were analyzed by modeling the volume fraction profiles $\phi_i(z)$ of all components in the system, namely the silicon substrate (i = Si), the silicon oxide layer ($i = SiO_2$), the initiator layer (i = init), the hydrated brush (i = b), and water (i = w). Here, z denotes the distance perpendicular to the substrate, with $z = 0$ defined at the substrate/brush interface. While the substrate, the silicon oxide, and the initiator layer were modeled as slabs of a given thickness, scattering length density, and roughness, a continuum description for the brush was opted. In particular, two approaches were used to model the volume fraction profile of the polymer brush. In the first one, the volume fraction profile of the brush is described by an analytical function depending on a restricted number of characteristic parameters;[18,74] in the second approach, the scattering length density profile is modeled without any *a priori* assumption on its shape.[75,76] Using well-defined analytical functions to model the brush conformations, as described by the first method, provides a means to link directly theoretical predictions with experiments, and the fitting procedures are generally numerically robust. In contrast, the form-free approach allows the experimentalist to explore the full brush conformational landscape at the cost of an associated risk of providing physically unreasonable solutions. Both approaches lead to comparable results (see Figure S5).

Polymer Brush Described with Analytical Expressions. To describe the polymer brush in swollen, collapsed, and intermediate states, the following analytical expression was used:

$$\phi_b(z) = \frac{\phi_i - \phi_o}{2}\,\mathrm{erfc}\left(\frac{z - z_i}{\sqrt{2}\,\sigma_i}\right) + k(z)\phi_o \exp\left[-\left(\frac{|z - z_o|}{\sigma_o}\right)^{\xi_o}\right] \tag{2}$$

The preceding expression models a relatively compact inner region by the error function, characterized by a degree of hydration (ϕ_i), an extension (z_i), and roughness (σ_i), and an outer region by a stretched exponential function, characterized by a stretching exponent (ξ_o), a degree of hydration (ϕ_o), an extension (z_0), and roughness (σ_o). Finally, the function

$$k(z) = 1 - \frac{1}{2}\,\mathrm{erfc}\left(\frac{z - z_i}{\sqrt{2}\,\sigma_i}\right) \tag{3}$$

ensures a smooth overlap between the inner and the outer region of the brush. To check that this function does not overdescribe the neutron reflectivity data, we modeled the volume fraction as a simple sigmoidal function as well, i.e., by fixing $k(z) = 0$ and $\phi_o = 0$. On the basis of the reduced χ^2 values (Figures S3 and S4), it can be stated that the two-region analytical expression does not overfit the data.

Polymer Brush Described with a Model-Free Approach. The model-free polymer brush profiles were obtained by interpolating a piecewise cubic Hermitian polynomial (PCHP) through four knots,[76] each characterized by its distance from the substrate and a brush volume fraction value. The choice of a PCHP allows us to enforce a monotonic decay of the polymer concentration from the substrate toward the solvent phase.[77]

In both cases, the volume fraction profiles are normalized such that $\int \phi_b\, dz = d_p$, with d_p being the amount of polymer expressed as volume of material per surface area, determined beforehand by optical ellipsometry. Finally, the scattering length density (SLD) profile of the system SLD(z) is calculated from the volume fraction profiles of the different components:

$$\mathrm{SLD}(z) = \sum_i \phi_i \mathrm{SLD}_i(z) \tag{4}$$

where SLD_i is the scattering length density of the ith component. The change of SLD as a function of pressure and temperature was considered using the specific densities and isothermal compressibility values determined by density and sound-velocity measurements. The used values are given in Tables S1−S3. Finally, the reflectivity curve was calculated using the Abeles matrix formalism upon discretization of the continuous profile into 1 Å thick slabs.

A bootstrap approach was used to estimate the uncertainty of the best fitting volume fraction profiles.[78] The procedure consists of generating N new data sets from the original experimental data, aimed

https://doi.org/10.1021/acs.macromol.2c01979
Macromolecules XXXX, XXX, XXX−XXX

at simulating N independent replicas of the measurement. In practice, for each experimental point, characterized by its average value R_i and standard deviation σ_{R_i}, N new values are sampled according to a normal distribution centered on R_i and with standard deviation σ_{R_i}. The new data are fitted with a perturbed set of initial values using the different models described in the article. The fitting procedure was performed using the differential evolution algorithm implemented in the LMFIT package. This procedure allows determining N different volume fraction profiles per data set and model—a representative case is shown in Figure S9. The average polymer volume fraction profile and its uncertainty are computed as the χ_{red}^{-2}-weighted average of the N different profiles obtained from the bootstrap analysis. The code used to fit the neutron reflectometry data is available upon request to the corresponding authors.

An in-depth analysis of the polymer brush profiles allows extracting the degree of hydration, the average brush thickness, and its roughness. In particular, the overlap integral is calculated as

$$I_{b,w} = \frac{1}{d_p}\int \phi_b(z)\phi_w(z)\,dz \tag{5}$$

This integral allows us to estimate the swelling of the polymer and varies between 0 for an anhydrous brush to 1 for an infinitely swollen brush. Moreover, the brush thickness d and roughness w are estimated using the following equations:[79]

$$d = 2Z_1 \tag{6}$$

$$w = 2Z_1\sqrt{\frac{3}{2}\frac{Z_2}{Z_1^2} - 2} \tag{7}$$

where Z_1 and Z_2 are the normalized first and second moment of the brush profile $\phi_b(z)$:

$$Z_1 = \frac{\int z\phi_b(z)\,dz}{\int \phi_b(z)\,dz} \tag{8}$$

$$Z_2 = \frac{\int z^2\phi_b(z)\,dz}{\int \phi_b(z)\,dz} \tag{9}$$

The advantage of this approach is that it allows for a direct comparison between any arbitrary profile with a brush exhibiting an error function profile with thickness d and roughness w and being characterized by the same zeroth, first, and second moment.

MD Simulations. Simulation Details. The simulated PNIPAM chains were 20 monomer units long with atactic stereochemistry. The modeling parameters for PNIPAM were taken from the OPLS-based force field by Palivec et al.,[16] whereas the SPC/E model[80] was used for simulating water.

The swollen state was modeled as a single stretched PNIPAM chain in a box of water, as shown in Figure 5i. The chain was restrained at both ends to fixed points in space by harmonic springs in order to maintain a stretched conformation. The collapsed, polymer-rich phase was modeled as a bulk of 48 aggregated PNIPAM chains in a cubic simulation box mixed with water (Figure 5(ii)). The number of water molecules per monomer was varied from n_w = 0.7 to 1.75 to simulate different hydration levels. Periodic boundary conditions in all three directions were used. The final results were averaged over 2−4 independent simulation runs with different starting configurations. The simulations were performed with the GROMACS 5.1 simulation package.[81] The Lennard-Jones (LJ) interactions were truncated at 1.0 nm. Electrostatic interactions were treated with particle-mesh-Ewald methods with a 1.0 nm real-space cutoff. The prescribed pressure was maintained with the Berendsen barostat with the time constant of 1 ps, and the box dimensions were tuned independently. The temperature in all simulations was set to 340 K (67 °C) with the velocity-rescaling thermostat with the time constant of 0.1 ps. The advantages of the higher temperature in the simulations compared with the experiments (25−45 °C) are considerably faster equilibration and available preexisting simulation trajectories at this temperature from our previous study.[49] Using a higher temperature should not alter the outcomes qualitatively, as the system does not undergo the coil-to-globule phase transition in the simulations.

Volume and Compressibility from Simulations. According to Euler's theorem, partial molar quantities are additive for homogeneous systems. Thus, we write the volumes per monomer in the swollen (s) and collapsed (c) states as the sum of the monomer volume and the water contribution

$$V^{(s)} = V_m^{(s)} + n_w^{(s)}V_w^0 \tag{10}$$

$$V^{(c)} = V_m^{(c)} + n_w^{(c)}V_w^{(c)} + (n_w^{(s)} - n_w^{(c)})V_w^0 \tag{11}$$

where $n_w^{(s)}$ and $n_w^{(c)}$ are the number of water molecules per monomer in the swollen and collapsed states, respectively. The volume of the collapsed state (eq 11) is composed of the volume of the polymer-rich phase (first two terms) and the water molecules released into the bulk water phase (third term). The difference in volume per monomer between the two states, $\Delta V = V^{(c)} - V^{(s)}$, is then

$$\Delta V = V_m^{(c)} - V_m^{(s)} + n_w^{(c)}(V_w^{(c)} - V_w^0) \tag{12}$$

which is the sum of the change in partial monomer volume (first two terms) and partial water volume per monomer (third term).

Taking the derivative of eq 12 with respect to pressure brings us to the corresponding compressibility factors

$$\Delta\kappa = \kappa_m^{(c)} - \kappa_m^{(s)} + n_w^{(c)}(\kappa_w^{(c)} - \kappa_w^0) \tag{13}$$

where $\kappa_i^{(s,c)} = -(\partial V_i^{(s,c)}/\partial P)_T$ is the partial compressibility factor of species i (m = monomer, w = water) in the swollen (s) or collapsed (c) state. The derivation generates also the term $(V_w^{(c)} - V_w^0)(\partial n_w^{(c)}/\partial P)_T$, which is negligible in our case, as we show in the Supporting Information.

The partial compressibility factors were obtained from additional simulations at an isotropic pressure of 1000 bar and then calculating the pressure derivatives using finite differences between the box volumes at 1000 and 1 bar, $\kappa \simeq -(\Delta V/\Delta P)_T$.

■ ASSOCIATED CONTENT

Supporting Information

The Supporting Information is available free of charge at https://pubs.acs.org/doi/10.1021/acs.macromol.2c01979.

Additional neutron reflectivity data and results, determination of polymer grafting density and molar mass, determination of the thermodynamic parameters of the swollen-to-collapsed phase transition, additional information about MD simulations (PDF)

■ AUTHOR INFORMATION

Corresponding Authors

Matej Kanduč − *Jožef Stefan Institute, SI-1000 Ljubljana, Slovenia;* orcid.org/0000-0002-5307-7488; Email: matej.kanduc@ijs.si

Leonardo Chiappisi − *Institut Max von Laue - Paul Langevin, 38042 Grenoble, France;* orcid.org/0000-0002-4594-2865; Email: chiappisil@ill.eu

Authors

Samantha Micciulla − *Institut Max von Laue - Paul Langevin, 38042 Grenoble, France*

Philipp Gutfreund − *Institut Max von Laue - Paul Langevin, 38042 Grenoble, France*

Complete contact information is available at: https://pubs.acs.org/10.1021/acs.macromol.2c01979

https://doi.org/10.1021/acs.macromol.2c01979
Macromolecules XXXX, XXX, XXX−XXX

Author Contributions

S.M. performed chemical synthesis of polymer brushes. S.M., P.G., and L.C. performed neutron reflectometry experiments. L.C. analyzed neutron reflectometry data. M.K. performed the MD simulations and data analysis. L.C. and M.K. designed the research. All authors wrote the manuscript.

Notes

The authors declare no competing financial interest.

■ ACKNOWLEDGMENTS

We thank Joachim Dzubiella for fruitful discussions. The ILL is acknowledged for the attribution of beam time on FIGARO (DOI:10.5291/ILL-DATA.9-11-1922) and granting access to the Partnership for Soft Condensed Matter (PSCM) laboratories, where the DSC, ellipsometry, density and sound-velocity measurements, and sample preparation were performed. We thank Roland Winter for lending the neutron reflectometry high-pressure cell to the ILL. M.K. acknowledges the financial support from the Slovenian Research Agency (Contracts P1-0055 and J1-1701).

■ REFERENCES

(1) Crespy, D.; Bozonnet, M.; Meier, M. 100 Years of Bakelite, the Material of a 1000 Uses. *Angew. Chem., Int. Ed.* **2008**, *47*, 3322−3328.
(2) Stuart, M. A. C.; Huck, W. T. S.; Genzer, J.; Müller, M.; Ober, C. K.; Stamm, M.; Sukhorukov, G. B.; Szleifer, I.; Tsukruk, V. V.; Urban, M.; Winnik, F. M.; Zauscher, S.; Luzinov, I.; Minko, S. Emerging applications of stimuli-responsive polymer materials. *Nat. Mater.* **2010**, *9*, 101−13.
(3) Hu, L.; Wan, Y.; Zhang, Q.; Serpe, M. J. Harnessing the Power of Stimuli-Responsive Polymers for Actuation. *Adv. Funct. Mater.* **2020**, *30*, 1903471.
(4) Chen, W.-L.; Cordero, R.; Tran, H.; Ober, C. K. 50th Anniversary Perspective: Polymer Brushes: Novel Surfaces for Future Materials. *Macromolecules* **2017**, *50*, 4089−4113.
(5) Scarpa, J. S.; Mueller, D. D.; Klotz, I. M. Slow hydrogen-deuterium exchange in a non-.alpha.-helical polyamide. *J. Am. Chem. Soc.* **1967**, *89*, 6024−6030.
(6) Heskins, M.; Guillet, J. E. Solution Properties of Poly(N-isopropylacrylamide). *Journal of Macromolecular Science: Part A - Chemistry* **1968**, *2*, 1441−1455.
(7) Abu-Lail, N. I.; Kaholek, M.; LaMattina, B.; Clark, R. L.; Zauscher, S. Micro-cantilevers with end-grafted stimulus-responsive polymer brushes for actuation and sensing. *Sens. Actuators, B* **2006**, *114*, 371−378.
(8) Halperin, A.; Kröger, M.; Winnik, F. M. Poly(N-isopropylacrylamide) Phase Diagrams: Fifty Years of Research. *Angewandte Chemie - International Edition* **2015**, *54*, 15342−15367.
(9) Fujishige, S.; Kubota, K.; Ando, I. Phase transition of aqueous solutions of poly(N-isopropylacrylamide) and poly(N-isopropylmethacrylamide). *J. Phys. Chem.* **1989**, *93*, 3311−3313.
(10) Kujawa, P.; Winnik, F. M. Volumetric Studies of Aqueous Polymer Solutions Using Pressure Perturbation Calorimetry: A New Look at the Temperature-Induced Phase Transition of Poly(N -isopropylacrylamide) in Water and D 2 O. *Macromolecules* **2001**, *34*, 4130−4135.
(11) Ding, Y.; Ye, X.; Zhang, G. Microcalorimetric Investigation on Aggregation and Dissolution of Poly(N -isopropylacrylamide) Chains in Water. *Macromolecules* **2005**, *38*, 904−908.
(12) Balu, C.; Delsanti, M.; Guenoun, P.; Monti, F.; Cloitre, M. Colloidal Phase Separation of Concentrated PNIPAm Solutions. *Langmuir* **2007**, *23*, 2404−2407.
(13) Wrede, O.; Reimann, Y.; Lülsdorf, S.; Emmrich, D.; Schneider, K.; Schmid, A. J.; Zauser, D.; Hannappel, Y.; Beyer, A.; Schweins, R.; Gölzhäuser, A.; Hellweg, T.; Sottmann, T. Volume phase transition kinetics of smart N-n-propylacrylamide microgels studied by time-resolved pressure jump small angle neutron scattering. *Sci. Rep.* **2018**, *8*, 13781.
(14) Kang, Y.; Joo, H.; Kim, J. S. Collapse−swelling transitions of a thermoresponsive, single poly (N-isopropylacrylamide) chain in water. *J. Phys. Chem. B* **2016**, *120*, 13184−13192.
(15) Tavagnacco, L.; Zaccarelli, E.; Chiessi, E. On the molecular origin of the cooperative coil-to-globule transition of poly(N -isopropylacrylamide) in water. *Phys. Chem. Chem. Phys.* **2018**, *20*, 9997−10010.
(16) Palivec, V.; Zadrazil, D.; Heyda, J.All-atom REMD simulation of poly-N-isopropylacrylamide thermodynamics in water: a model with a distinct 2-state behavior. *arXiv***2018**, arXiv:1806.05592 (accessed 2022-05-22).
(17) Penfold, J.; Thomas, R. K. The application of the specular reflection of neutrons to the study of surfaces and interfaces. *J. Phys.: Condens. Matter* **1990**, *2*, 1369−1412.
(18) Murdoch, T. J.; Humphreys, B. A.; Willott, J. D.; Gregory, K. P.; Prescott, S. W.; Nelson, A.; Wanless, E. J.; Webber, G. B. Specific Anion Effects on the Internal Structure of a Poly(N-isopropylacrylamide) Brush. *Macromolecules* **2016**, *49*, 6050−6060.
(19) Ishida, N.; Biggs, S. Direct Observation of the Phase Transition for a Poly(N -isopropylacryamide) Layer Grafted onto a Solid Surface by AFM and QCM-D. *Langmuir* **2007**, *23*, 11083−11088.
(20) Futscher, M. H.; Philipp, M.; Müller-Buschbaum, P.; Schulte, A. The Role of Backbone Hydration of Poly(N-isopropyl acrylamide) Across the Volume Phase Transition Compared to its Monomer. *Sci. Rep.* **2017**, *7*, 17012.
(21) Yaminsky, V. V.; Vogler, E. A. Hydrophobic hydration. *Curr. Opin. Colloid Interface Sci.* **2001**, *6*, 342−349.
(22) Zeman, L.; Patterson, D. Pressure effects in polymer solution phase equilibria. II. Systems showing upper and lower critical solution temperatures. *J. Phys. Chem.* **1972**, *76*, 1214−1219.
(23) Smeller, L. Pressure−temperature phase diagrams of biomolecules. *Biochimica et Biophysica Acta (BBA) - Protein Structure and Molecular Enzymology* **2002**, *1595*, 11−29.
(24) Chen, M.; Briscoe, W. H.; Armes, S. P.; Klein, J. Lubrication at Physiological Pressures by Polyzwitterionic Brushes. *Science* **2009**, *323*, 1698−1701.
(25) Aertsen, A.; Meersman, F.; Hendrickx, M. E.; Vogel, R. F.; Michiels, C. W. Biotechnology under high pressure: applications and implications. *Trends Biotechnol.* **2009**, *27*, 434−441.
(26) Teixeira, S. C. High-pressure small-angle neutron scattering for food studies. *Curr. Opin. Colloid Interface Sci.* **2019**, *42*, 99−109.
(27) Tavagnacco, L.; Chiessi, E.; Zaccarelli, E. Molecular insights on poly (N-isopropylacrylamide) coil-to-globule transition induced by pressure. *Phys. Chem. Chem. Phys.* **2021**, *23*, 5984−5991.
(28) Lee, H.; Son, S. H.; Sharma, R.; Won, Y.-Y. A Discussion of the pH-Dependent Protonation Behaviors of Poly(2-(dimethylamino)-ethyl methacrylate) (PDMAEMA) and Poly(ethylenimine- ran −2-ethyl-2-oxazoline) (P(EI- r -EOz)). *J. Phys. Chem. B* **2011**, *115*, 844−860.
(29) Bochenek, S.; Camerin, F.; Zaccarelli, E.; Maestro, A.; Schmidt, M. M.; Richtering, W.; Scotti, A. In-situ study of the impact of temperature and architecture on the interfacial structure of microgels. *Nat. Commun.* **2022**, *13*, 3744.
(30) Yim, H.; Kent, M. S.; Satija, S.; Mendez, S.; Balamurugan, S. S.; Balamurugan, S.; Lopez, G. P. Evidence for vertical phase separation in densely grafted, high-molecular-weight poly(N-isopropylacrylamide) brushes in water. *Phys. Rev. E* **2005**, *72*, 051801.
(31) Varma, S.; Bureau, L.; Débarre, D. The Conformation of Thermoresponsive Polymer Brushes Probed by Optical Reflectivity. *Langmuir* **2016**, *32*, 3152−3163.
(32) Niebuur, B.-J.; Chiappisi, L.; Zhang, X.; Jung, F.; Schulte, A.; Papadakis, C. M. Formation and Growth of Mesoglobules in Aqueous Poly(N -isopropylacrylamide) Solutions Revealed with Kinetic Small-Angle Neutron Scattering and Fast Pressure Jumps. *ACS Macro Lett.* **2018**, *7*, 1155−1160.
(33) Grobelny, S.; Hofmann, C. H.; Erlkamp, M.; Plamper, F. A.; Richtering, W.; Winter, R. Conformational changes upon high

https://doi.org/10.1021/acs.macromol.2c01979
Macromolecules XXXX, XXX, XXX−XXX

pressure induced hydration of poly(N-isopropylacrylamide) microgels. *Soft Matter* **2013**, *9*, 5862.
(34) Ballauff, M.; Borisov, O. V. Phase transitions in brushes of homopolymers. *Polymer* **2016**, *98*, 402−408.
(35) Niebuur, B.-J.; Claude, K.-L.; Pinzek, S.; Cariker, C.; Raftopoulos, K. N.; Pipich, V.; Appavou, M.-S.; Schulte, A.; Papadakis, C. M. Pressure-Dependence of Poly(N -isopropylacrylamide) Mesoglobule Formation in Aqueous Solution. *ACS Macro Lett.* **2017**, *6*, 1180−1185.
(36) Meersman, F.; Wang, J.; Wu, Y.; Heremans, K. Pressure effect on the hydration properties of poly(N-isopropylacrylamide) in aqueous solution studied by FTIR spectroscopy. *Macromolecules* **2005**, *38*, 8923−8928.
(37) Hawley, S. A. Reversible pressure-temperature denaturation of chymotrypsinogen. *Biochemistry* **1971**, *10*, 2436−2442.
(38) Shibayama, M.; Isono, K.; Okabe, S.; Karino, T.; Nagao, M. SANS Study on Pressure-Induced Phase Separation of Poly(N-isopropylacrylamide) Aqueous Solutions and Gels. *Macromolecules* **2004**, *37*, 2909−2918.
(39) Niskanen, J.; Wu, C.; Ostrowski, M.; Fuller, G. G.; Hietala, S.; Tenhu, H. Thermoresponsiveness of PDMAEMA. Electrostatic and Stereochemical Effects. *Macromolecules* **2013**, *46*, 2331−2340.
(40) Ravindra, R.; Winter, R. On the temperature - Pressure free-energy landscape of proteins. *ChemPhysChem* **2003**, *4*, 359−365.
(41) Smirnovas, V.; Winter, R.; Funck, T.; Dzwolak, W. Thermodynamic Properties Underlying the α-Helix-to-β-Sheet Transition, Aggregation, and Amyloidogenesis of Polylysine as Probed by Calorimetry, Densimetry, and Ultrasound Velocimetry. *J. Phys. Chem. B* **2005**, *109*, 19043−19045.
(42) Rubens, P.; Heremans, K. Pressure-temperature gelatinization phase diagram of starch: An in situ Fourier transform infrared study. *Biopolymers* **2000**, *54*, 524−530.
(43) Kunugi, S.; Takano, K.; Tanaka, N.; Suwa, K.; Akashi, M. Effects of Pressure on the Behavior of the Thermoresponsive Polymer Poly(N -vinylisobutyramide) (PNVIBA). *Macromolecules* **1997**, *30*, 4499−4501.
(44) Kato, E. Thermodynamic study of a pressure-temperature phase diagram for poly(N-isopropylacrylamide) gels. *J. Appl. Polym. Sci.* **2005**, *97*, 405−412.
(45) Graziano, G. On the temperature-induced coil to globule transition of poly-N-isopropylacrylamide in dilute aqueous solutions. *Int. J. Biol. Macromol.* **2000**, *27*, 89−97.
(46) Meersman, F.; Wang, J.; Wu, Y.; Heremans, K. Pressure Effect on the Hydration Properties of Poly(N -isopropylacrylamide) in Aqueous Solution Studied by FTIR Spectroscopy. *Macromolecules* **2005**, *38*, 8923−8928.
(47) Reinhardt, M.; Dzubiella, J.; Trapp, M.; Gutfreund, P.; Kreuzer, M.; Gröschel, A. H.; Müller, A. H. E.; Ballauff, M.; Steitz, R. Fine-Tuning the Structure of Stimuli-Responsive Polymer Films by Hydrostatic Pressure and Temperature. *Macromolecules* **2013**, *46*, 6541−6547.
(48) Tavagnacco, L.; Zaccarelli, E.; Chiessi, E. Modeling Solution Behavior of Poly(N -isopropylacrylamide): A Comparison between Water Models. *J. Phys. Chem. B* **2022**, *126*, 3778−3788.
(49) Kanduč, M.; Kim, W. K.; Roa, R.; Dzubiella, J. Selective Molecular Transport in Thermo-Responsive Polymer Membranes: Role of Nanoscale Hydration and Fluctuations. *Macromolecules* **2018**, *51*, 4853−4864.
(50) Kanduč, M.; Kim, W. K.; Roa, R.; Dzubiella, J. How the Shape and Chemistry of Molecular Penetrants Control Responsive Hydrogel Permeability. *ACS Nano* **2021**, *15*, 614−624.
(51) Onori, G.; Santucci, A. Dynamical and structural properties of water/alcohol mixtures. *J. Mol. Liq.* **1996**, *69*, 161−181.
(52) Onori, G. Adiabatic compressibility and structure of aqueous solutions of ethyl alcohol. *J. Chem. Phys.* **1988**, *89*, 4325−4332.
(53) Reddy, V. K.; Reddy, K. S.; Krishnaiah, A. Excess volumes, speeds of sound, and viscosities for mixtures of 1, 2-ethanediol and alkoxy alcohols with water at 308.15 K. *J. Chem. Eng.* **1994**, *39*, 615−617.
(54) Douhéret, G.; Davis, M.; Høiland, H. Speeds of sound and excess volumetric properties of mixtures of water with ethylene glycol monopropyl ether at 298.15 K. *J. Mol. Liq.* **1999**, *80*, 1−18.
(55) Wang, H.; Wu, Y.; Dong, W. A study of densities and volumetric properties of binary mixtures containing nitrobenzene at T = (293.15 to 353.15) K. *J. Chem. Thermodyn* **2005**, *37*, 866−886.
(56) Seemann, H.; Winter, R.; Royer, C. A. Volume, expansivity and isothermal compressibility changes associated with temperature and pressure unfolding of staphylococcal nuclease. *J. Mol. Biol.* **2001**, *307*, 1091−1102.
(57) Collins, M. D.; Hummer, G.; Quillin, M. L.; Matthews, B. W.; Gruner, S. M. Cooperative water filling of a nonpolar protein cavity observed by high-pressure crystallography and simulation. *Proc. Natl. Acad. Sci. U. S. A.* **2005**, *102*, 16668−16671.
(58) Rasaiah, J. C.; Garde, S.; Hummer, G. Water in nonpolar confinement: From nanotubes to proteins and beyond. *Annu. Rev. Phys. Chem.* **2008**, *59*, 713−740.
(59) Mittal, J.; Hummer, G. Static and dynamic correlations in water at hydrophobic interfaces. *Proc. Natl. Acad. Sci. U. S. A* **2008**, *105*, 20130−20135.
(60) Sarupria, S.; Garde, S. Quantifying water density fluctuations and compressibility of hydration shells of hydrophobic solutes and proteins. *Phys. Rev. Lett.* **2009**, *103*, 037803.
(61) Rego, N. B.; Patel, A. J. Understanding hydrophobic effects: Insights from water density fluctuations. *Annual Review of Condensed Matter Physics* **2022**, *13*, 303−324.
(62) Tripathy, M.; Bharadwaj, S.; van der Vegt, N. F. Characterizing polymer hydration shell compressibilities with the small-system method. *Nanomaterials* **2020**, *10*, 1460.
(63) Aliotta, F.; Gapiński, J.; Pochylski, M.; Ponterio, R.; Saija, F.; Salvato, G. Excess compressibility in binary liquid mixtures. *J. Chem. Phys.* **2007**, *126*, 224508.
(64) Marcus, Y.; Hefter, G. The compressibility of liquids at ambient temperature and pressure. *J. Mol. Liq.* **1997**, *73*, 61−74.
(65) Roche, J.; Royer, C. A. Lessons from pressure denaturation of proteins. *Journal of The Royal Society Interface* **2018**, *15*, 20180244.
(66) Matyjaszewski, K.; Xia, J. Atom Transfer Radical Polymerization. *Chem. Rev.* **2001**, *101*, 2921−2990.
(67) Fujie, T.; Park, J. Y.; Murata, A.; Estillore, N. C.; Tria, M. C. R.; Takeoka, S.; Advincula, R. C. Hydrodynamic transformation of a freestanding polymer nanosheet induced by a thermoresponsive surface. *ACS Appl. Mater. Interfaces* **2009**, *1*, 1404−13.
(68) Zhou, F.; Zheng, Z.; Yu, B.; Liu, W.; Huck, W. T. S. Multicomponent Polymer Brushes. *J. Am. Chem. Soc.* **2006**, *128*, 16253−16258.
(69) Cisse, A.; Peters, J.; Lazzara, G.; Chiappisi, L. PyDSC: a simple tool to treat differential scanning calorimetry data. *J. Therm. Anal. Calorim.* **2021**, *145*, 403−409.
(70) Balestri, A.; Chiappisi, L.; Montis, C.; Micciulla, S.; Lonetti, B.; Berti, D. Organized Hybrid Molecular Films from Natural Phospholipids and Synthetic Block Copolymers: A Physicochemical Investigation. *Langmuir* **2020**, *36*, 10941−10951.
(71) Campbell, R.; Wacklin, H.; Sutton, I.; Cubitt, R.; Fragneto, G. FIGARO: The new horizontal neutron reflectometer at the ILL. *European Physical Journal Plus* **2011**, *126*, 107.
(72) Jeworrek, C.; Steitz, R.; Czeslik, C.; Winter, R. High pressure cell for neutron reflectivity measurements up to 2500 bar. *Rev. Sci. Instrum.* **2011**, *82*, 025106.
(73) Gutfreund, P.; Saerbeck, T.; Gonzalez, M. A.; Pellegrini, E.; Laver, M.; Dewhurst, C.; Cubitt, R. Towards generalized data reduction on a chopper-based time-of-flight neutron reflectometer. *J. Appl. Crystallogr.* **2018**, *51*, 606−615.
(74) Field, J. B.; Toprakcioglu, C.; Ball, R. C.; Stanley, H. B.; Dai, L.; Barford, W.; Penfold, J.; Smith, G.; Hamilton, W. Determination of End-Adsorbed Polymer Density Profiles by Neutron Reflectometry. *Macromolecules* **1992**, *25*, 434−439.
(75) Galvin, C. J.; Dimitriou, M. D.; Satija, S. K.; Genzer, J. Swelling of Polyelectrolyte and Polyzwitterion Brushes by Humid Vapors. *J. Am. Chem. Soc.* **2014**, *136*, 12737−12745.

https://doi.org/10.1021/acs.macromol.2c01979
Macromolecules XXXX, XXX, XXX−XXX

(76) Gresham, I. J.; Murdoch, T. J.; Johnson, E. C.; Robertson, H.; Webber, G. B.; Wanless, E. J.; Prescott, S. W.; Nelson, A. R. J. IUCr, Quantifying the robustness of the neutron reflectometry technique for structural characterization of polymer brushes. *J. Appl. Crystallogr.* **2021**, *54*, 739−750.
(77) Fritsch, F. N.; Carlson, R. E. Monotone Piecewise Cubic Interpolation. *SIAM Journal on Numerical Analysis* **1980**, *17*, 238−246.
(78) Navarro Pérez, R.; Amaro, J.; Ruiz Arriola, E. Bootstrapping the statistical uncertainties of NN scattering data. *Physics Letters B* **2014**, *738*, 155−159.
(79) Habicht, J.; Schmidt, M.; Rühe, J.; Johannsmann, D. Swelling of Thick Polymer Brushes Investigated with Ellipsometry. *Langmuir* **1999**, *15*, 2460−2465.
(80) Berendsen, H. J. C.; Grigera, J. R.; Straatsma, T. P. The Missing Term in Effective Pair Potentials. *J. Phys. Chem.* **1987**, *91*, 6269−6271.
(81) van der Spoel, D.; Lindahl, E.; Hess, B.; Groenhof, G.; Mark, A. E.; Berendsen, H. J. C. GROMACS: Fast, Flexible, and Free. *J. Comput. Chem.* **2005**, *26*, 1701−1718.

https://doi.org/10.1021/acs.macromol.2c01979
Macromolecules XXXX, XXX, XXX−XXX